JPE 18-5-10

https://doi.org/10.6113/JPE.2018.18.5.1398
ISSN(Print): 1598-2092 / ISSN(Online): 2093-4718

# Double Vector Based Model Predictive Torque Control for SPMSM Drives with Improved Steady-State Performance

Xiaoguang Zhang[†,*], Yikang He[*], and Benshuai Hou[**]

[†]Inverter Technologies Engineering Research Center of Beijing,
North China University of Technology, Beijing, China
[*]Collaborative Innovation Center of Key Power Energy-Saving Technologies in Beijing,
North China University of Technology, Beijing, China
[**]Beijing Shougang International Engineering Technology Co., Ltd, Beijing, China

## Abstract

In order to further improve the steady-state control performance of model predictive torque control (MPTC), a double-vector-based model predictive torque control without a weighting factor is proposed in this paper. The extended voltage vectors synthesized by two basic voltage vectors are used to increase the number of feasible voltage vectors. Therefore, the control precision of the torque and the stator flux along with the steady-state performance can be improved. To avoid testing all of the feasible voltage vectors, the solution of deadbeat torque control is calculated to predict the reference voltage vector. Thus, the candidate voltage vectors, which need to be evaluated by a cost function, can be reduced based on the sector position of the predicted reference voltage vector. Furthermore, a cost function, which only includes a reference voltage tracking error, is designed to eliminate the weighting factor. Moreover, two voltage vectors are applied during one control period, and their durations are calculated based on the principle of reference voltage tracking error minimization. Finally, the proposed method is tested by simulations and experiments.

**Key words:** Model predictive torque control, Surface mounted permanent-magnet synchronous motor (SPMSM), Weighting factor

## I. INTRODUCTION

Recently, model predictive torque control (MPTC) has been widely researched and applied in motor drives as a high dynamic performance control strategy [1]-[4]. MPTC methods can be classified into two categories, i.e., continuous control set MPTC [5] and finite control set MPTC [6]. The continuous control set MPTC adopts space vector modulation (SVM) to obtain a desired voltage vector, which is predicted by calculating an open-loop optimal solution. Unlike the continuous control set MPTC, finite control set MPTC predicts system behaviors based on the inherent discrete nature of the motor inverter. Then the voltage vector evaluated by the torque and flux error based cost function, which can obtain optimal predictive behavior, is directly applied to the motor without modulation. Therefore, finite control set MPTC has the advantages of an intuitive concept, easy implement and multi-objective control ability [7]-[10].

However, there are some key challenges that need to be faced in MPTC methods, such as high computation burden and high current ripple [11]. In the conventional MPTC, all of the feasible voltage vectors need to be tested by a cost function to select the best one, which leads to an increase of the calculating time and restricts the application of multistep prediction [12]-[14]. On the other hand, in conventional MPTC methods, only one voltage vector is selected to apply to the motor in one control period, which results in poor steady-state control performance, i.e., high torque and current ripple, and

Manuscript received Dec. 15, 2017; accepted Apr. 2, 2018
Recommended for publication by Associate Editor Dong-Hee Lee.
[†]Corresponding Author: zxg@ncut.edu.cn
Tel: +86-010-8880-2691, North China University of Technology
[*]Collaborative Innovation Center of Key Power Energy-Saving Technologies in Beijing, North China University of Technology, China
[**]Beijing Shougang International Engineering Tech. Co., Ltd, China

a variable switching frequency when compared with SVM-based methods [15], [16]. Therefore, in order to obtain satisfactory steady-state performance, the sampling frequency of the conventional MPTC has to be increased.

To reduce the computational burden of MPTC, some improved methods have been presented, such as sphere decoding methods [17], [18] and the binary search tree algorithm [19]. These methods have the advantages of easy implementation and a low calculation burden because the optimization process is pre-solved offline. However, in practical applications, it is difficult to obtain a real optimal solution using the aforementioned offline methods due to changes in the operation conditions. Therefore, the online methods, which have the capability of real-time optimization to reduce the computation burden, are proposed in [20]. In this method, the number of candidate voltage vectors in the conventional MPTC are reduced from seven to three based on the principle of deadbeat predictive control. However, the steady-state performance is not improved.

In order to reduce the current ripple in the MPTC method and to improve the steady-state control performance, some methods have been presented recently. Vector duty cycle based MPTC methods were proposed in [21]-[23]. In these methods, two voltage vectors, including a nonzero voltage vector and a null zero voltage vector, are selected in one control period. The durations of the nonzero vector and the null vector are calculated based on some principles, such as torque ripple minimization and torque deadbeat. To further reduce the current ripples of MPTC, a method where two nonzero voltage vectors are adopted during one control period was reported in [24]-[26]. The steady-state performance can be improved. This is especially true when the motor operates at a high speed. Although duty cycle based MPTC methods can improve the steady-state control performance, a weighting factor is still needed to balance the control of the torque and stator flux. Therefore, the tedious tuning work of the weighting factor is inevitable. On the other hand, a long prediction horizon can also be adopted to achieve a reduction of the current ripples [27]. However, in long prediction horizon based MPTC methods, when the predictive step increases, the number of the candidate voltage vectors also increases. This results in a further increase in the computation burden. This means that a contradictory issue between an improvement of the steady-state performance and an increase of the computation burden exists in long prediction horizon based MPTC methods.

To further improve the steady-state control performance of the conventional MPTC, a novel MPTC method is proposed in this paper. The extended voltage vectors, which are synthesized by two basic voltage vectors, together with the basic voltage vectors are served as candidate voltage vectors (fourteen vectors). To avoid testing all of the candidate voltage vectors, the solution of the deadbeat torque control is calculated to predict the reference voltage vector from all of the feasible voltage vectors. Thus, the number of candidate voltage vectors can be reduced from fourteen to one according to the sector position of the reference voltage vector. Furthermore, a reference voltage tracking error based cost function is designed to evaluate the candidate voltage vectors. Information of the torque error and flux error is included in the reference voltage vector tracking error. Therefore, the weighting factor in the conventional MPTC is avoided. Moreover, in this paper, two voltage vectors are applied during one control period and their durations are calculated. Finally, the proposed method is tested by simulations and experiments.

## II. SPMSM Mathematical Model

Omitting the complicated and tedious derivation process, the SPMSM mathematical model in synchronous rotating frame can be described as follows [28], [29]:

$$u_s = A \cdot i_s + B \cdot \psi_s + C \cdot \frac{d\psi_s}{dt} \tag{1}$$

$$\psi_s = D \cdot i_s + E \tag{2}$$

$$T_e = \frac{3}{2} p \psi_f i_q \tag{3}$$

where $u_s=[u_d, u_q]^T$, $i_s=[i_d, i_q]^T$, $\psi_s=[\psi_d, \psi_q]^T$ and:

$$A=\begin{bmatrix} R_s & 0 \\ 0 & R_s \end{bmatrix}, \quad B=\begin{bmatrix} 0 & -\omega \\ \omega & 0 \end{bmatrix}, \quad C=\begin{bmatrix} 1 & 0 \\ 0 & 1 \end{bmatrix}, \quad D=\begin{bmatrix} L_d & 0 \\ 0 & L_q \end{bmatrix},$$

$$E=\begin{bmatrix} \psi_f \\ 0 \end{bmatrix}.$$

In this model, $u_d$ and $u_q$ are the stator voltages, $i_d$ and $i_q$ are the stator currents, $\psi_d$ and $\psi_q$ are the d-axis and q-axis flux linkage, $L_d=L_q=L$ is the stator inductance, $R_s$ is the stator resistance, $\psi_f$ is the permanent magnets flux linkage, and $\omega$ is the electrical rotor velocity (rad/s) .

## III. Principle of the Proposed MPTC Method

The control program of the proposed MPTC method mainly includes four parts, i.e. the desired voltage vector prediction and vector selection, the torque and flux prediction, the vector duration calculation and the pulse generation, as shown as Fig. 1. In this method, the output of the speed controller is served as the reference value of the electromagnetic torque, and the reference value of the stator flux is obtained by the MTPA algorithm based on the reference value of the electromagnetic torque [30]. The details of this method will be elaborated in the following subsection.

### *A. Extended Voltage Vectors*

In this paper, a two-level three-phase inverter is used, which has eight basic switching states, including six nonzero

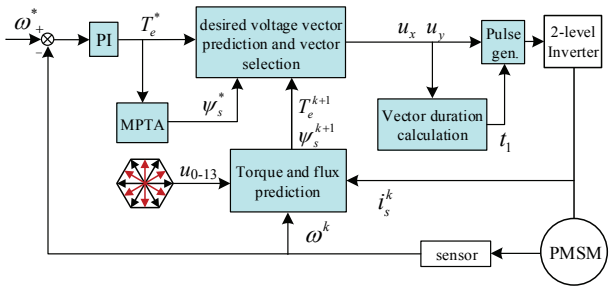


Fig. 1. Control diagram of the proposed MPTC method.

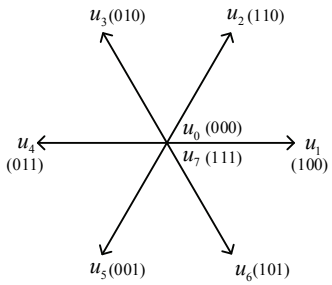


Fig. 2. Basic voltage vector of a two-level inverter.

voltage vectors ($u_1$,$u_2$,...,$u_6$) and two zero vectors ($u_0$, $u_7$), as shown in Fig. 2. The conventional model predictive control selects a voltage vector that is able to minimize the cost function as the optimal vector among the eight basic voltage vectors in each control period. However, due to the number limitation on the basic voltage vectors, the steady-state control performance of the conventional model predictive control is unsatisfactory. Although duty cycle optimization [31]-[33] can be introduced to the model predictive control to improve the steady-state performance, the influence caused by the number limitation of the feasible voltage vectors still exists.

To further improve the steady-state performance in the model predictive control, the six extended voltage vectors are synthesized by two adjacent basic nonzero voltage vectors. Therefore, the number of all the feasible voltage vectors in the model predictive control can be increased up to fourteen. Fig. 3 shows the distribution of the basic voltage vectors and the extended voltage vectors. In this paper, one control period is subdivided into two equal parts. Then the extended voltage vectors ($u_8$, $u_9$,..., $u_{13}$) can be expressed as follows:

$$u_{j+7} = \frac{T_s}{2}u_j + \frac{T_s}{2}u_{j+1} \tag{4}$$

where, $j$ = 1, 2 . . . , 6 represents the available voltage vectors, and $T_s$ is a control period. According to the principle of the model predictive control, the 14 voltage vectors must be used to predict the system behavior of the next control period. They must also be evaluated by the cost function to select the best one. This leads to an increase in the calculation burden of the control system. Therefore, it is necessary to develop a pre-selection method to reduce the computation time.

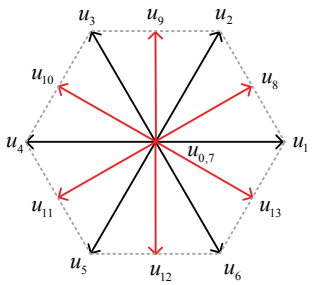


Fig. 3. Vector distribution of the basic voltage vectors and the extended voltage vectors.

### *B. Desired Voltage Vector Prediction*

In order to reduce the computational burden, a deadbeat direct torque and flux control (DB-DTFC) algorithm is adopted to predict the desired voltage vector, which is used as the reference voltage vector for all of the feasible voltage vectors to reduce the selection range of the candidate voltage vector.

According to the motor models (1), (2) and (3), a change of torque, i.e., the item $T_e^{k+1} - T_e^k$, can be expressed as [34]:

$$T_e^{k+1} - T_e^k = \frac{3p\psi_f}{2L}\left(u_q^k T_s - \frac{R_s T_s \psi_q^k}{L} - \omega T_s \psi_d^k\right) \tag{5}$$

On the other hand, since the effect of the stator resistance can be negligible, the relationship between the stator flux and the voltage can be approximated as follows:

$$\begin{aligned}(\psi_s^{k+1})^2 &= (\psi_d^{k+1})^2 + (\psi_q^{k+1})^2 \\ &= (u_d^k T_s + \psi_d^k + \omega T_s \psi_q^k)^2 + (u_q^k T_s + \psi_q^k - \omega T_s \psi_d^k)^2\end{aligned} \tag{6}$$

According to the principle of the DB-DTFC algorithm, the torque value at the (k+1)th instant and the stator flux at the (k+1)th instant (i.e., $T_e^{k+1}$ and $\psi_s^{k+1}$) should be set to reference commands to obtain the expected response of the torque and stator flux in next control period. Thus, by combining equations (5) and (6), the solution of DB-DTFC is obtained as:

$$\begin{cases} u_d^k = \dfrac{-X_1 \pm \sqrt{X_1^2 - X_2}}{T_s} \\ u_q^k = \dfrac{B}{T_s} \end{cases} \tag{7}$$

where:

$$X_1 = \psi_d^k + \omega \psi_q^k T_s$$

$$X_2 = B^2 + 2B(\psi_q^k - \omega \psi_d^k T_s) + (\psi_d^k)^2 + (\psi_q^k)^2 + \omega^2 T_s^2[(\psi_d^k)^2 + (\psi_q^k)^2] - (\psi_s^*)^2$$

$$B = \frac{2L}{3p\psi_f}(T_e^* - T_e^k) + \frac{R_s T_s \psi_q^k}{L} + \omega T_s \psi_d^k.$$

Therefore, the angle of the predicted reference voltage vector can be calculated according to (8) by transforming the solution of equation (7) to the αβ frame.

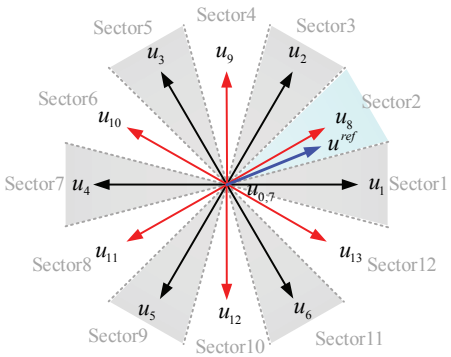


Fig. 4. Sector partition.

$$\theta_{\text{ref}} = \arctan\left(\frac{u_\beta^k}{u_\alpha^k}\right). \tag{8}$$

### C. Candidate Vectors Selection

For the double-vector-based MPTC method, the main works are the selection of two vectors and the calculation of their respective durations in one control period. In this paper, like the conventional double-vector-based MPTC method, the first voltage vector should select a nonzero voltage vector. However, in the proposed method, the number of all the feasible voltage vectors increases due to the added extended vectors when compared with the conventional MPTC, which means that the computation burden of the proposed method increases. Therefore, in order to reduce the selection range of the first nonzero voltage vector, the whole α-β plane is divided into 12 sectors, as shown as Fig. 4. There is only one nonzero voltage vector in each sector. Therefore, the first nonzero voltage vector can be selected according to the sector of the desired voltage vector (8). For example, if the sector of the desired voltage vector ($u_{ref}$) is 2 during the current control period, as shown as Fig. 4, the voltage vector $u_8$ should be selected as the first nonzero voltage vector. This avoids testing all of the feasible voltage vectors in each control period.

When the first voltage vector is selected according to the sector position, the candidate voltage vectors of the second voltage vector can be determined based on the principle of avoiding a high switching frequency. This means two nonzero voltage vectors, which are adjacent to the selected first voltage vector, and a zero voltage vector are considered as the candidate voltage vectors of the second voltage vector. Suppose $u_j$ (j=1, 2, ...13) is selected as the first voltage vector, then the candidate vectors of the second voltage vector should include $u_{j-1}$, $u_{j+1}$ and the zero vector $u_{0,7}$.

### D. Cost Function Design

After obtaining the candidate voltage vector, the next step is to determine the optimal voltage vectors and their durations. In this paper, the voltage tracking error based cost function is designed as follows:

$$g = \left|u_{dref} - u_{di}\right|^2 + \left|u_{qref} - u_{qi}\right|^2 + I_{\lim} \tag{9}$$

where $u_{\text{dref}}$ and $u_{\text{qref}}$ are the solutions of the DB-DTFC, i.e., the desired voltage vector. In addition, $u_{\text{di}}$ and $u_{\text{qi}}$ represent the candidate voltage vectors, which need to be tested by the cost function. Furthermore, $I_{\text{lim}}$ represents the current protection, which is shown as:

$$I_{\lim} = \begin{cases} 0 & (|i(k+2)| \le |i_{\max}|) \\ \infty & (|i(k+2)| > |i_{\max}|) \end{cases} \tag{10}$$

In (9), based on the mathematic models (1), (2) and (3), the d-axis and q-axis voltage error can be derived as:

$$\begin{aligned} \left|u_{\text{dref}} - u_{di}\right| &= \left|\frac{d\psi_d^*}{dt} - \omega\psi_q^* - \frac{d\psi_d^i}{dt} + \omega\psi_q^i\right| \\ &= \left|\frac{d}{dt}\left(\psi_d^* - \psi_d^i\right) - \omega\left(\psi_q^* - \psi_q^i\right)\right| \end{aligned} \tag{11}$$

$$\begin{aligned} \left|u_{\text{qref}} - u_{qi}\right| &= \left|Ri_q^* + \frac{d\psi_q^*}{dt} + \omega\psi_d^* - Ri_q^i - \frac{d\psi_q^i}{dt} - \omega\psi_d^i\right| \\ &= \left|\frac{2R}{3p\psi_f}T_e^* + \frac{d\psi_q^*}{dt} + \omega\psi_d^* - \frac{2R}{3p\psi_f}T_e^i - \frac{d\psi_q^i}{dt} - \omega\psi_d^i\right| \\ &= \left|\frac{2R}{3p\psi_f}\left(T_e^* - T_e^i\right) + \frac{d}{dt}\left(\psi_q^* - \psi_q^i\right) + \omega\left(\psi_d^* - \psi_d^i\right)\right| \end{aligned} \tag{12}$$

where $T_e^i$, $\psi_d^i$ and $\psi_q^i$ represent the predictive torque and stator flux of the tested voltage vector, respectively. Then the voltage tracking error based cost function (9) can be expressed based on the torque prediction error and the flux prediction error, which is shown as follows:

$$\begin{aligned} g = &\left|\frac{d}{dt}\left(\psi_d^* - \psi_d^i\right) - \omega\left(\psi_q^* - \psi_q^i\right)\right|^2 \\ &+ \left|\frac{2R}{3p\psi_f}\left(T_e^* - T_e^i\right) + \frac{d}{dt}\left(\psi_q^* - \psi_q^i\right) + \omega\left(\psi_d^* - \psi_d^i\right)\right|^2 \end{aligned} \tag{13}$$

Its discrete form is:

$$\begin{aligned} g = &\left|\begin{aligned} &\frac{\psi_d^*(k+2) - \psi_d^i(k+2)}{T_s} - \frac{\psi_d^*(k+1) - \psi_d^i(k+1)}{T_s} \\ &-\omega(k)\left[\psi_q^*(k+1) - \psi_q^i(k+1)\right] \end{aligned}\right|^2 \\ &+ \left|\begin{aligned} &\frac{2R}{3p\psi_f}\left[T_e^*(k+1) - T_e^i(k+1)\right] + \frac{\psi_q^*(k+2) - \psi_q^i(k+2)}{T_s} \\ &- \frac{\psi_q^*(k+1) - \psi_q^i(k+1)}{T_s} + \omega(k)\left[\psi_d^*(k+1) - \psi_d^i(k+1)\right] \end{aligned}\right|^2 \end{aligned} \tag{14}$$

According to (13) and (14), it can be seen that similar to the cost function of the conventional MPTC, the control targets of the cost function (9) are also the torque error and stator flux error. However, unlike the conventional MPTC, the cost function (9) can avoid the use of a weighting factor. The control balance between the torque and the stator flux is automatically implemented based on the present operating condition.

### E. Vector Duration Determination

Assume that the first voltage vector and the second voltage vector are $u_x$ and $u_y$, respectively, and that their durations are $t_1$ and $T_s$-$t_1$. Then the cost function (9) can be expressed as:

$$g = \left| u_{\text{ref}} - \frac{t_1}{T_s} u_x - \frac{(T_s - t_1)}{T_s} u_y \right|^2 \tag{15}$$

Equation (15) should be minimized to obtain the optimal control performance of the torque and stator flux. By solving $\partial g/\partial t_1=0$, the optimal time of the first voltage vector and the second voltage vector are obtained as:

$$\begin{cases} t_1 = \dfrac{\left(u_y - T_s u_{\text{ref}}\right) \cdot \left(u_y - u_x\right)}{\left(u_y - u_x\right)^2} \\ t_2 = T_s - t_1 \end{cases} \tag{16}$$

It should be noted that there are three kinds of possible vector combinations for the selected two vectors in this paper. The time-assignment principle of the vector is described as following.

1). When the two voltage vectors selected by the cost function are a basic voltage and a zero voltage vector, their vector durations are the same as (16).

2). When the two voltage vectors selected by the cost function are a basic voltage vector and an extended voltage vector, their vector durations need to be reassigned according to (16). This is due to the fact that the extended voltage vector is synthesized by two basic voltage vectors. For example, the selected two vectors are a basic voltage vector $u_1$ and an extended voltage vector $u_8$, as shown as Fig. 4, and their durations are $t_1$ and $t_2$ calculated by (16). The first voltage vector selects the basic vector $u_1$ and the second voltage vector $u_8$ is synthesized by the basic vectors $u_1$ and $u_2$ based on the (4). Thus, the real voltage vectors applied for the motor are the basic vectors $u_1$ and $u_2$. Then according to (16), the durations of the basic vectors $u_1$ and $u_2$ can be obtained by:

$$\begin{cases} t_{u_1} = t_1 + \dfrac{t_2}{2} = t_1 + \dfrac{T_s - t_1}{2} = \dfrac{T_s + t_1}{2} \\ t_{u_2} = \dfrac{t_2}{2} = \dfrac{T_s - t_1}{2} \end{cases} \tag{17}$$

3). When the two voltage vectors selected by the cost function are an extended voltage vector and a zero voltage vector. For example, the first voltage vector is the extended voltage vector $u_8$ and the second voltage vector is a zero vector. According to (4), the vector $u_8$ is synthesized by the basic vectors $u_1$ and $u_2$. Thus, the real voltage vectors applied to the motor include three vectors, i.e., the basic vectors $u_1$ and $u_2$ along with the zero vector $u_{0(7)}$. Then according to (4) and (16), the durations of these three vectors can be obtained by:

$$\begin{cases} t_{u_1} = \dfrac{t_1}{2} \\ t_{u_2} = \dfrac{t_1}{2} \\ t_{u_0} = T_s - t_1 \end{cases} \tag{18}$$

After selecting the two voltage vectors and calculating their durations, the drive pulses for all of the power switches in a two-level three-phase inverter can be generated. It should be noted that the two zero vectors ($u_0$ and $u_7$) should be selected reasonably to reduce the switch times. For example, if the voltage vector $u_1$(100) is selected, then vector $u_0$(000) rather than $u_7$(111) should be followed.

## IV. Experimental Results

In this section, experiments on the proposed MPTC method in a SPMSM system were carried out. In the experiment, the prior two-vector-based MPTC [35] and the proposed MPTC method were tested under the same test conditions and the same sampling frequency 20kHz. The motor parameters are listed in Table I. For simplicity, the prior method in [35] is named as MPTC-I, and the proposed MPTC method is named as MPTC-II.

Fig. 5, 6 and 7 present steady-state performance of both methods at low speed (200r/min), medium speed (1000r/min) and high speed (2000r/min) with a rated load. From top to bottom, the curves are the stator flux, torque and stator current, respectively. In addition, the corresponding harmonic spectrums of the stator current at low, medium and high speeds are shown in Fig 8, 9 and 10.

At a speed of 200r/min, current THD analysis results under the control of the MPTC-I is 6.16%, while the current THD of the proposed MPTC-II is 5.21%. At a medium speed of 1000r/min and a rated speed of 2000r/min, the current THD analysis results under the control of the MPTC-I are 9.97% and 14.17%, respectively. However, the current THD results of the proposed MPTC-II method are reduce to 7.63% and 12.53%, respectively. This means that the current THD of the proposed method is lower than that of the MPTC-I method. In order to illustrate the universality of these results, current THD analysis results of both methods at various speeds are shown in Fig. 11. It can be seen that the proposed MPTC-II method has better steady-state control performance when compared with the MPTC-I.

Apart from the steady-state performance comparison, dynamic response comparisons of both methods are shown in Figs. 12 and 13. Fig. 12 shows curves of speed, stator flux, torque and phase current, when speed step changes from 200r/min to 2000r/min without a load. These experimental results demonstrate that the prior MPTC-I and the proposed MPTC-II can both achieve fast and non-overshoot speed tracking control without large torque fluctuations. In addition,

TABLE I
PARAMETERS OF THE SPMSM

| | |
|---|---|
| d- and q-axes inductances | $L_d$ =$L_q$ =11mH |
| Stator phase resistance | $R$ =3Ω |
| Rated speed | $n_N$ =2000r/min |
| Number of pole pairs | $P$ =3 |
| Rotational inertia | $J$ =0.00129kg·m2 |
| Flux linkage of permanent magnets | $\psi_a$ =0.35Wb |
| Rated torque | 6N.m |
| Rated current | 2.69A |
| Power | 1.25kW |

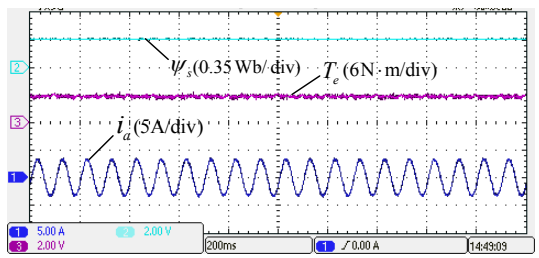


(a)

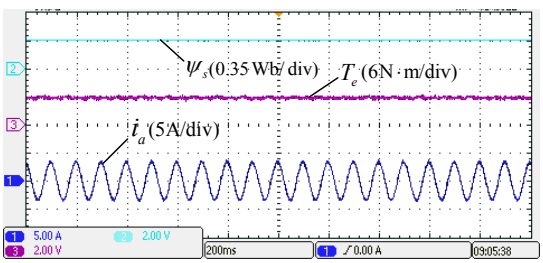


(b)

Fig. 5. Steady-state experimental results under the control of two methods at a low speed of 200r/min and rated load: (a) The prior MPTC-I, (b) The proposed MPTC-II.

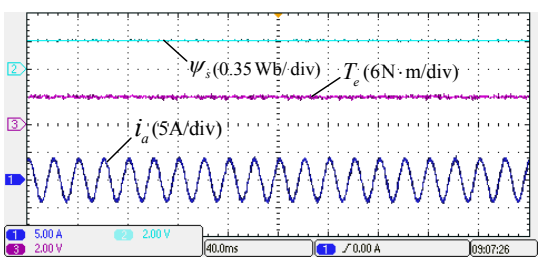


(a)

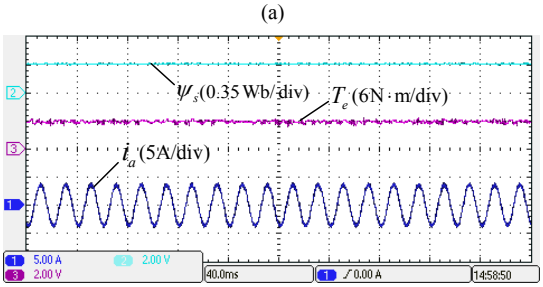


(b)

Fig. 6. Steady-state experimental results under the control of two methods at a medium speed of 1000r/min and rated load: (a) The prior MPTC-I, (b) The proposed MPTC-II.

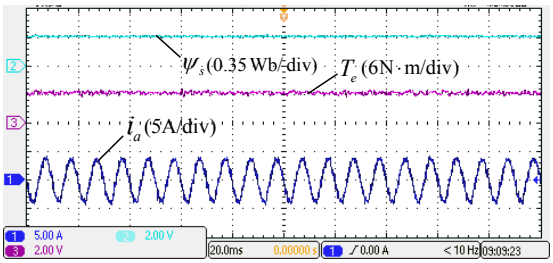


(a)

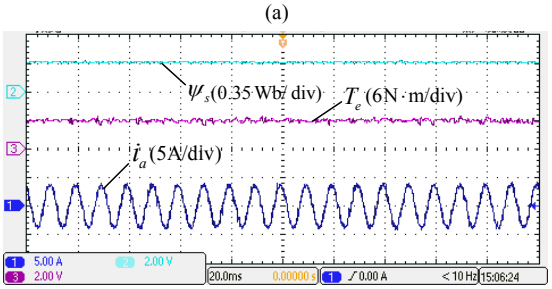


(b)

Fig. 7. Steady-state experimental results under the control of two methods at a high speed of 2000r/min and rated load: (a) The prior MPTC-I, (b) The proposed MPTC-II.

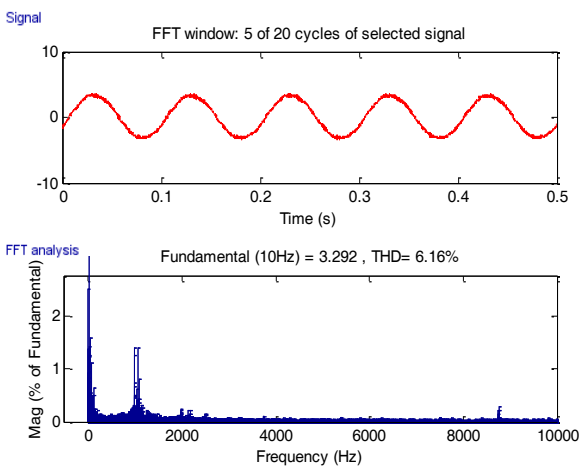


(a)

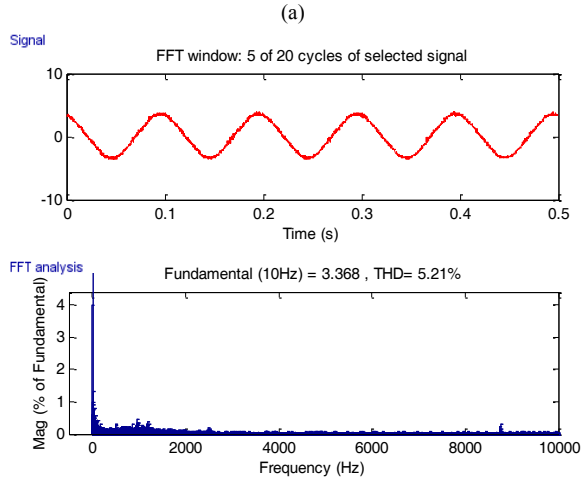


(b)

Fig. 8. Current THD analysis results under the control of two methods at a low speed of 200r/min and rated load: (a) The prior MPTC-I, (b) The proposed MPTC-II.

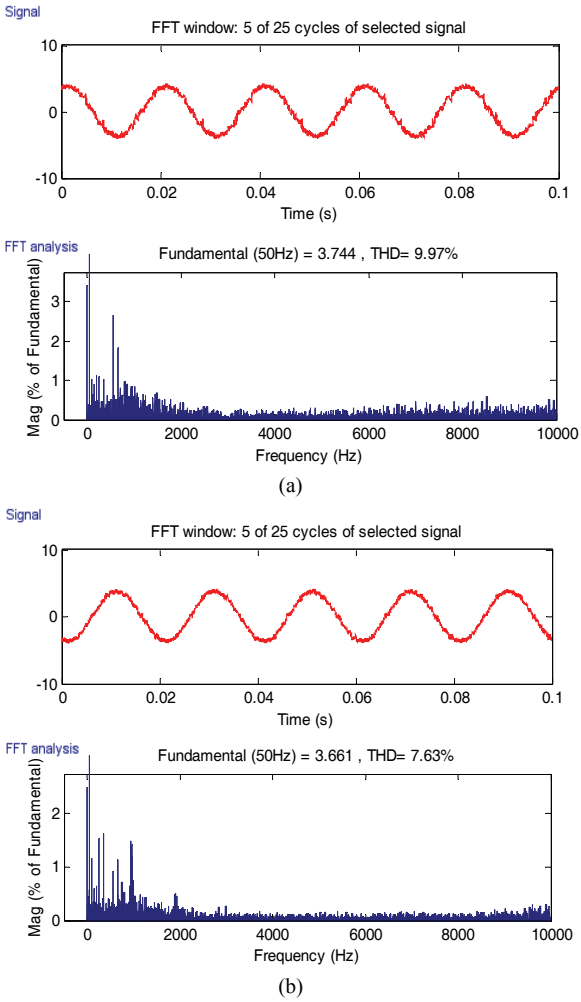


Fig. 9. Current THD analysis results under the control of two methods at a medium speed of 1000r/min and rated load: (a) The prior MPTC-I, (b) The proposed MPTC-II.

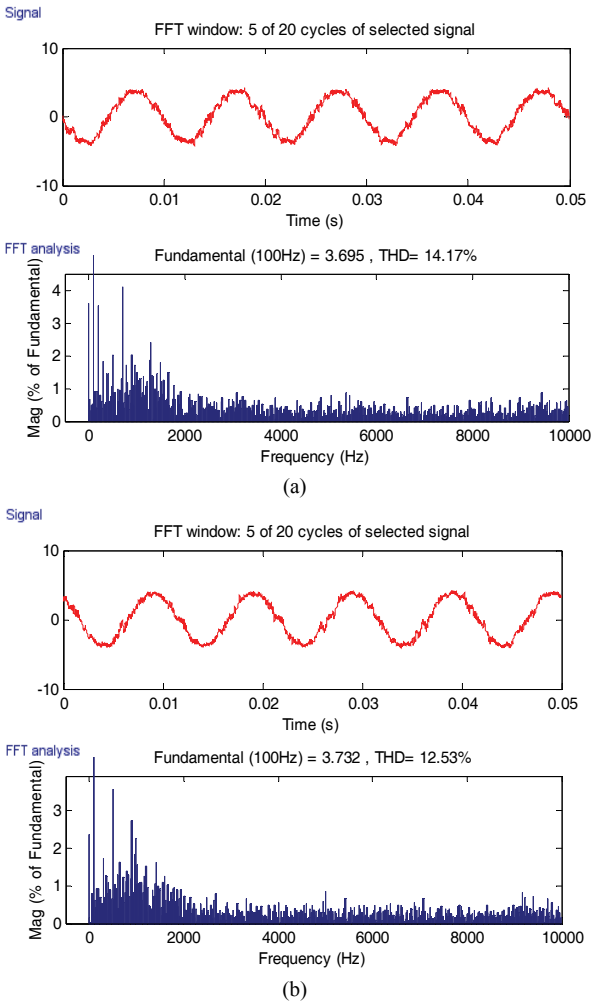


Fig. 10. Current THD analysis results under the control of two methods at a high speed of 2000r/min and rated load: (a) The prior MPTC-I, (b) The proposed MPTC-II.

the dynamic responses of the MPTC-I and the proposed MPTC-II are compared in Fig. 13, when the motor load is suddenly changed from 0 to the rated value. It is clearly seen that the motor speed can be recovered to its reference value quickly, which means that both methods can obtain satisfactory dynamic response and excellent external disturbance rejection performance.

From the result comparison of both methods, it can be seen that the proposed MPTC-II method inherits the conventional advantage of model predictive control, i.e., a quick dynamic response, while improving on the steady-state control performance. Therefore, the proposed MPTC-II method is more attractive in practical applications.

The switching frequencies of the MPTC-I and the proposed MPTC-II method are illustrated in Fig. 14. It can be seen that when compared with the MPTC-I, the switching frequency of the proposed MPTC-II is roughly constant, and that introducing an extended voltage vector slightly increases the switching frequency. In order to further evaluate the proposed MPTC-II method, a current THD analysis comparison

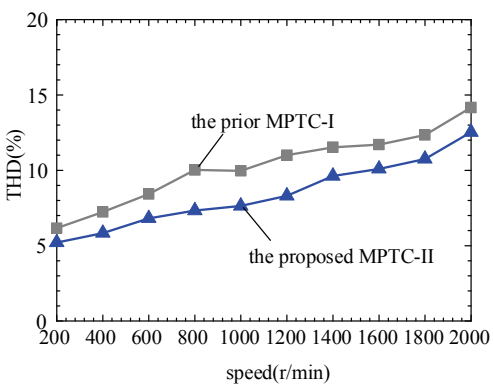


Fig. 11. Current THD analysis results of both methods at various speeds.

between the MPTC-I and the proposed MPTC-II at the same switching frequency is shown in Fig. 15. To achieve a fair comparison, the switching frequency of the prior MPTC-I method is used as the reference to modify the sampling frequency of the proposed MPTC-II method. This is

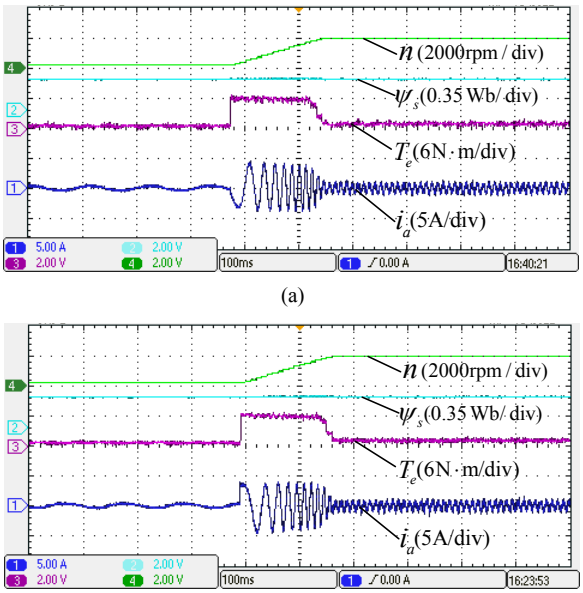


Fig. 12. Dynamic test of two methods when the speed reference step changes from 200r/min to 2000r/min: (a) The prior MPTC-I: (b) The proposed MPTC-II.

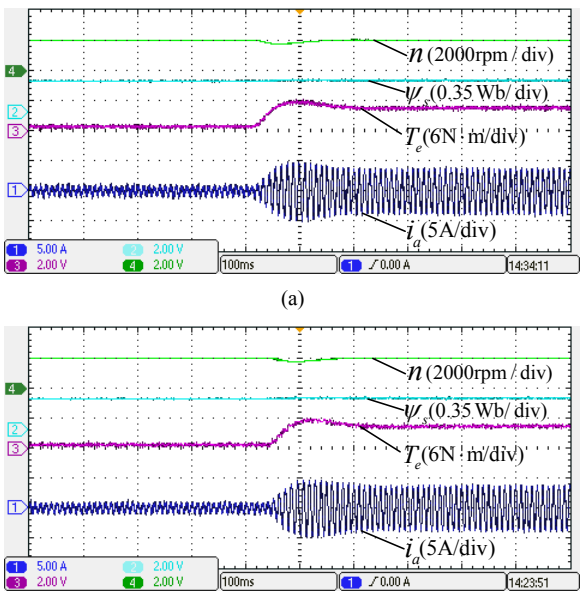


Fig. 13. Dynamic test of two methods when the load step changes from zero to rated value: (a) The prior MPTC-I, (b) The proposed MPTC-II.

considered as common practice and standard when different control methods need to be compared, as shown in [36]. From Fig. 15, it can be seen that under the condition of similar switching frequencies, the current THD of the proposed MPTC-II is still smaller than that of the prior MPTC-I method at different speeds. This further demonstrates that the proposed MPTC-II method has better steady-state control performance when compared with the prior MPTC-I method.

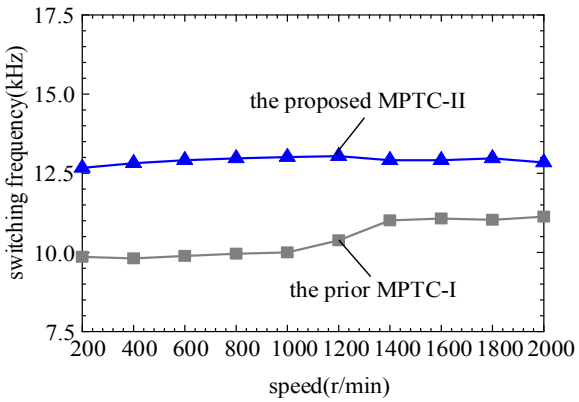


Fig. 14. Average switching frequency of both methods.

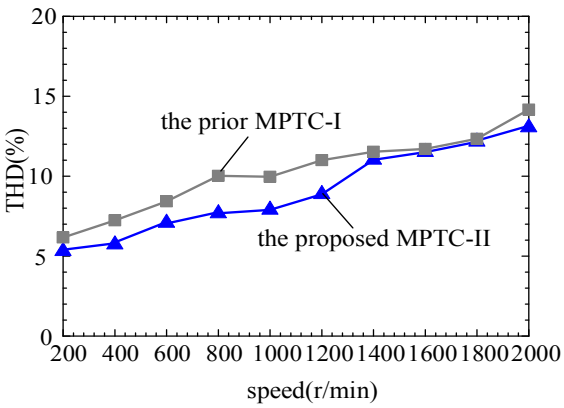


Fig. 15. Current THD comparison of both methods at the same average switching frequency.

In summary, the above results demonstrate that the proposed method inherits the advantage of a fast dynamic response from the conventional MPTC and improves the steady-state performance.

In order to evaluate the influence of parameter variations on the control performance, experimental results under the control of the proposed method are shown in Fig. 16, where the machine parameters, including the resistance, inductance and permanent magnets flux linkage, are increased by 50% at a speed of 1000r/min. According to Fig. 16, it can be seen that resistance variations have no obvious influence on the control performance. It can also be seen that the inductance variation increases the torque and current ripple a little. In addition, from Fig. 16(d), it can be seen that although variation of the permanent magnets flux linkage causes torque/current ripple increases and generates a tracking error of the flux linkage, the whole control system works well. This shows that the proposed method has some robustness against parameter variations.

Finally, a comparison of calculation times under the control of both methods is listed in Table II. It can be seen that that the proposed method need a little more time than the prior method.

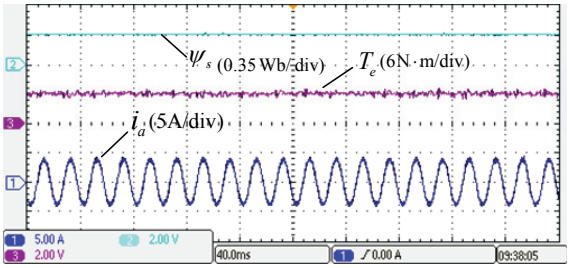


(a)

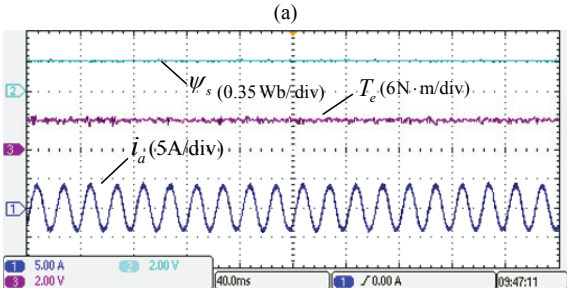


(b)

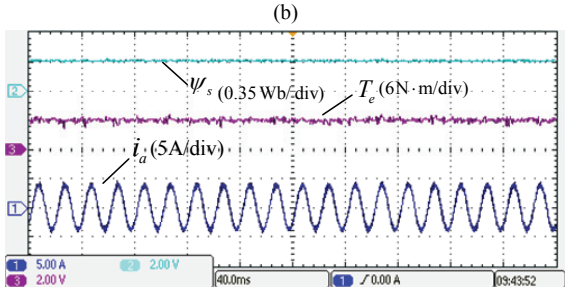


(c)

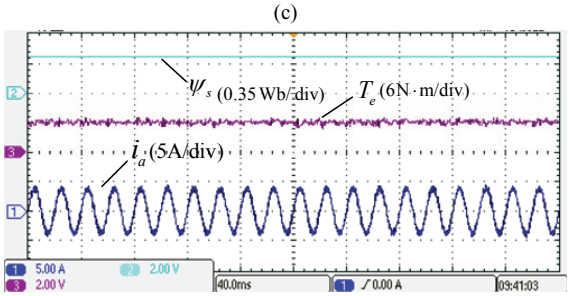


(d)

Fig. 16. Experimental results of the MPTC-II method with machine parameter variations: (a) Without machine parameter variations; (b) When the resistance increases 50%; (c) When the inductance increases 50%; (d) When the permanent magnets flux linkage increases 50%.

TABLE II
CALCULATION TIME OF BOTH METHODS

| Method | the prior MPTC-I | the proposed MPTC-II |
|---|---|---|
| Times($us$) | 40.51 | 40.76 |

## V. CONCLUSIONS

In this paper, an improved MPTC method has been presented and experimentally applied to a SPMSM system. This paper includes two major contributions. 1) An extended voltage vector is introduced to increase the number of the candidate voltage vectors and the control precision of the torque and stator flux is improved. 2) An extended voltage vector based MPTC method without a weighting factor is proposed, in which two voltage vectors are applied during one control period and an improvement of the steady-state control performance is achieved. In addition, the elimination of the weighting factor between the torque and the stator flux further increases the practicality of the MPTC method.

## ACKNOWLEDGMENT

This work was sponsored in part by the National Natural Science Foundation of China under Grants #51507004, by the Beijing Natural Science Foundation under Grants #3172011, by the research funds for the State Key Laboratory of Automotive Safety and Energy under Project No. KF1824, by the Young Top-Notch Talents Program of Beijing Excellent Talents Funding (2017000026833ZK12), and the Outstanding Young Scholars Fund of North China University of Technology.

## REFERENCES

[1] T. Geyer, G. Papafotiou, and M. Morari, "Model predictive direct torque control-part I: Concept, algorithm, and analysis," *IEEE Trans. Ind. Electron*., Vol. 56, No. 6, pp. 1894-1905, Jun. 2009.

[2] X. Zhang, B. Hou, and Y. Mei, "Deadbeat predictive current control of permanent magnet synchronous motors with stator current and disturbance observer," *IEEE Trans. Power Electron*., Vol. 32, No. 5, pp. 3818-3834, May 2017.

[3] G. Zhang, G. Wang, D. Xu, and N. Zhao, "ADALINE-network-based PLL for position sensorless interior permanent magnet synchronous motor drives," *IEEE Trans. Power Electron*., Vol. 31, No. 2, pp. 1450-1460, Feb., 2016.

[4] Y. Wang, X. Wang, W. Xie, F. Wang, M. Dou, R. M. Kennel, R. D. Lorenz, and D. Gerling, "Deadbeat model predictive torque control with discrete space vector modulation for PMSM drives," *IEEE Trans. Ind. Electron*., Vol.64, No.5, pp. 3537-3547, May 2017.

[5] S. Mariethoz, A. Domahidi, and M. Morari, "High-bandwidth explicit model predictive control of electrical drives," *IEEE Trans. Ind. Appl*., Vol. 48, No.6, pp. 1980-1992, Nov./Dec. 2012.

[6] S. Kouro, P. Cortes, R. Vargas, U. Ammann, and J. Rodriguez, "Model predictive control-a simple and powerful method to control power converters," *IEEE Trans. Ind. Electron*., Vol.56, No.6, pp. 1826-1838, Jun. 2009.

[7] Z. Xiang, X. Zhu, L. Quan, Y. Du, C. Zhang, and D. Fan, "Multi-level design optimization and operation of a brushless double mechanical ports flux-switching permanent magnet motor," *IEEE Trans. Ind. Electron*., Vol. 63, No. 10, pp. 6042-6054, Oct. 2016.

[8] H. Miranda, P. Cortes, J. Yuz, and J. Rodriguez, "Predictive torque control of induction machines based on state-space models," *IEEE Trans. Ind. Electron*., Vol. 56, No.6, pp. 1916-1924, Jun. 2009.

[9] C. A. Rojas, J. Rodriguez, F. Villarroel, J. R. Espinoza, C. A. Silva, and M. Trincado, "Predictive torque and flux control without weighting factors," *IEEE Trans. Ind. Electron*., Vol. 60, No. 2, pp. 681-690, Jul. 2013.

[10] Z. Zhou, C. Xia, Y. Yan, Z. Wang, and T. Shi, "Torque ripple minimization of predictive torque control for PMSM with extended control set," *IEEE Trans. Ind. Electron*., Vol. 64, No. 9, pp. 6930-6939, Sep. 2017.

[11] Y. Zhang and H. Yang, "Current prediction based zero sequence current suppression strategy for the semicontrolled open-winding PMSM generation system with a common DC bus," *IEEE Trans. Ind. Electron*., Vol. 65, No. 8, pp. 6066-6076, Aug. 2018.

[12] D. Casadei, F. Profumo, G. Serra, and A. Tani, "FOC and DTC: two viable schemes for induction motors torque control," *IEEE Trans. Power Electron*., Vol. 17, No. 5, pp. 779-787, Sep. 2002.

[13] G. Foo and M. F. Rahman, "Sensorless direct torque and flux-controlled IPM synchronous motor drive at very low speed without signal injection," *IEEE Trans. Ind. Electron*., Vol. 57, No. 1, pp. 395-403, Jan. 2010.

[14] P. Stolze, M. Tomlinson, R. Kennel, and T. Mouton, "Heuristic finite-set model predictive current control for induction machines," in *Proc. IEEE Energy Conv. Congr. Expo*, pp. 1221-1226, 2013.

[15] L. Tarisciotti, P. Zanchetta, A. Watson, S. Bifaretti, and J. C. Clare, "Modulated model predictive control for a seven-level cascaded hbridge back-to-back converter," *IEEE Trans. Ind. Electron*., Vol. 61, No. 10, pp. 5375-5383, Oct. 2014.

[16] P. Karamanakos, P. Stolze, R. M. Kennel, S. Manias, and H. du Toit Mouton, "Variable switching point predictive torque control of induction machines," *IEEE J. Emerg. Sel. Topics Power Electron*., Vol. 2, No. 2, pp. 285-295, Jun. 2014.

[17] T. Geyer and D. E. Quevedo, "Performance of multistep finite control set model predictive control for power electronics," *IEEE Trans. Power Electron*., Vol. 30, No. 3, pp. 1633-1644, Mar. 2015.

[18] T. Geyer and D. E. Quevedo, "Multistep finite control set model predictive control for power electronics," *IEEE Trans. Power Electron*., Vol. 29, No. 12, pp. 6836-6846, Dec. 2014.

[19] A. Linder and R. Kennel, "Model predictive control for electrical drives," in *Proc. IEEE 36th Power Electron. Specialists Conf*., Jun. 2005, pp. 1793-1799.

[20] X. Wei, W. Xiaocan, W. Fengxiang, X. Wei, R. M. Kennel, D. Gerling, and R. D. Lorenz, "Finite-control-set model predictive torque control with a deadbeat solution for pmsm drives," *IEEE Trans. Ind. Electron*., Vol. 62, No. 9, pp. 5402-5410, Sep. 2015.

[21] M. Pacas and J. Weber, "Predictive direct torque control for the pm synchronous machine," *IEEE Trans. Ind. Electron*., Vol. 52, No. 5, pp. 1350-1356, Oct. 2005.

[22] E. Flach, R. Hoffmann, and P. Mutschler, "Direct mean torque control of an induction motor," in *Eur. Conf. Power Electron. and Appl*., Vol. 3, pp. 3.672-3.677, 1997.

[23] S. Alireza Davari, D. A. Khaburi, and R. Kennel, "An improved fcs-mpc algorithm for an induction motor with an imposed optimized weighting factor," *IEEE Trans. Power Electron*., Vol. 27, No. 3, pp. 1540-1551, Mar. 2012.

[24] P. Landsmann and R. Kennel, "Saliency-based sensorless predictive torque control with reduced torque ripple," *IEEE Trans. Power Electron*., Vol. 27, No. 10, pp. 4311-4320, Oct. 2012.

[25] L. Tarisciotti, P. Zanchetta, A. Watson, S. Bifaretti, and J. C. Clare, "Modulated model predictive control for a seven-level cascaded h-bridge back-to-back converter," *IEEE Trans. Ind. Electron*., Vol. 61, No. 10, pp. 5375-5383, Oct. 2014.

[26] P. Karamanakos, P. Stolze, R. M. Kennel, S. Manias, and H. du Toit Mouton, "Variable switching point predictive torque control of induction machines," *IEEE J. Emerg. and Sel. Topics Power Electron*., Vol. 2, No. 2, pp. 285-295, Jun. 2014.

[27] T. Geyer and D. Quevedo, "Performance of multistep finite control set model predictive control for power electronics," *IEEE Trans. Power Electron*., Vol. 30, No. 3, pp. 1633-1644, Apr. 2015.

[28] Y. Shi, K. Sun, L. Huang and Y. Li, "Online identification of permanent magnet flux based on extended Kalman filter for IPMSM drive with position sensorless control," *IEEE Trans. Ind. Electron*. Vol. 59, No. 11, pp. 4169-4178, Nov. 2012.

[29] G. Wang, H. Zhan, G. Zhang, X. Gui, and D. Xu., "Adaptive compensation method of position estimation harmonic error for EMF-based observer in sensorless IPMSM drives," *IEEE Trans. Power Electron.*, Vol. 29, No.6, pp. 3055-3064, Jun. 2014.

[30] M. Nemec, D. Nedeljkovic, and V. Ambrozic, "Predictive torque control of induction machines using immediate flux control," *IEEE Trans. Ind. Electron*., Vol. 54, No. 4, pp. 2009-2017, Aug. 2007.

[31] Y. Zhang and J. Zhu, "Direct torque control of permanent magnet synchronous motor with reduced torque ripple and commutation frequency," *IEEE Trans. Power Electron*., Vol. 26, No. 1, pp. 235-248, Jan. 2011.

[32] J.-K. Kang and S.-K. Sul, "New direct torque control of induction motor for minimum torque ripple and constant switching frequency," *IEEE Trans. Ind. Appl*., Vol. 35, No. 5, pp. 1076-1082, Sep./Oct. 1999.

[33] K.-K. Shyu, J.-K. Lin, V.-T. Pham, M.-J. Yang, and T.-W. Wang, "Global minimum torque ripple design for direct torque control of induction motor drives," *IEEE Trans. Ind. Electron*., Vol. 57, No. 9, pp. 3148-3156, Sep. 2010.

[34] J. S. Lee, C.-H. Choi, J.-K. Seok, and R. D. Lorenz, "Deadbeat-direct torque and flux control of interior permanent magnet synchronous machines with discrete time stator current and stator flux linkage observer," *IEEE Trans. Ind. Appl*., Vol. 47, No. 4, pp. 1749-1758, May. 2011.

[35] X. Zhang and B. Hou, "Double vectors model predictive torque control without weighting factor based on voltage tracking error," *IEEE Trans. Power Electron*., Vol.33, No. 3, pp. 2368-2380, Mar. 2018.

[36] F. Morel, X. Lin-Shi, J.-M. Retif, B. Allard, and C. Buttay, "A comparative study of predictive current control schemes for a permanent-magnet synchronous machine drive," *IEEE Trans. Ind. Electron*., Vol. 56, No. 7, pp. 2715-2728, Jul. 2009.

**Xiaoguang Zhang** received his B.S. degree in Electrical Engineering from the Heilongjiang Institute of Technology, Harbin, China, in 2007; and his M.S. and Ph.D. degrees in Electrical Engineering from the Harbin Institute of Technology, Harbin, China, in 2009 and 2014, respectively. He is presently working as a Distinguished Professor at the North China University of Technology, Beijing, China. From 2012 to 2013, he was a Research Associate at the Wisconsin Electric Machines and Power Electronics Consortium (WEMPEC), University of Wisconsin–Madison, Madison, WI, USA. His current research interests include power electronics and electric machines drives.

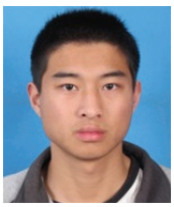

**Yikang He** was born in Hubei, China, in 1993. He received his B.S. degree in Electrical Engineering from the North China University of Technology, Beijing, China, in 2016, where he is presently working towards his M.S. degree. His current research interest include permanent magnet synchronous motor drives.

**Benshuai Hou** was born in Shandong, China, in 1989. He received his B.S. degree in Electrical Engineering from Beijing Union University, Beijing, China, in 2013. He is presently working towards his M.S. degree at the North China University of Technology, Beijing, China. His current research interests include permanent magnet machine drives.